International Electronic Journal of Pure and Applied Mathematics

Volume 4 No. 4 2012, 230-261

HEAT AND MASS TRANSFER OVER A STRETCHING SHEET IN POROUS MEDIA IN A ROTATING SYSTEM WITH HALL CURRENTS

M. Kinyanjui[1], K. Giterere[2] §, S.M. Uppal[3]

[1,2,3]P.O. Box 62000-00200
Nairobi, KENYA

Abstract: In this work, finite difference method is applied to study unsteady hydromagnetic boundary-layer flow Newtonian fluid due to a stretching sheet in a rotating system. The heat and mass transfer, and Hall currents have been investigated. The sheet is embedded in a uniform porous medium and is subjected to transverse magnetic field that cuts perpendicularly across the flow. The coupled non-linear partial differential equations governing the flow field have been solved numerically using the finite difference method. The influence of non-dimensional parameters on the flow field are discussed in detail, viz. the Reynolds number Re, Prandtl number Pr, Eckert Number Ec, Magnetic parameter M, the Hall parameter m, the injection parameter w_o, Joule heating parameter N, Radiation parameter R, Permeability constant K, Rotational parameter R_o, local temperature Grashof number Gr_θ, the local mass Grashof number Gr_c, Schmidt number Sc and Soret number Sr. The method of Least Squares is used to study the effect of changing some of these parameters on the skin-friction coefficients, rate of mass transfer and local wall heat flux. The resulting velocity, temperature and concentration profiles are presented graphically. A change in the parameters is observed to either increase, decrease or to have no effect on the velocity, temperature, and concentration profiles respectively.

AMS Subject Classification: 00A69
Key Words: magnetohydrodynamics, natural convection, boundary layer, radiation, joule heating, Coriolis force, Hall currents, and ion-slip currents

Received: June 8, 2011

§Correspondence author

International Electronic Journal of Pure and Applied Mathematics – IEJPAM, Volume 4, No. 4 (2012)

1. Introduction

The Hall and ion-slip currents are significant in MHD flows involving partially ionized gases e.g. water gas seeded with potassium. In an ionized gas where the density is low and/or the magnetic field is very strong, the effects of Hall and ion-slip currents affect the velocity profiles significantly. The problem of heat source is important for it has applications in areas such as effective cooling of electronic equipment. The study of MHD flows with Hall and ion-slip currents has important applications in engineering problems such as MHD generators, Hall accelerators, flight magnetohydrodynamics, etc. The ion-slip currents have been neglected. Kinyanjui, et al. (1998) also studied the MHD Stokes problem for a vertical infinite plate in a dissipative rotating fluid with Hall current. Kinyanjui, et al. (2001) presented some work on MHD free convection heat and mass transfer of a heat generating fluid past an impulsively started infinite porous plate with Hall current and radiation absorption. Ram (1991) analysed the effects of Hall currents on the combined thermal and mass diffusion effects through a porous medium in a rotating system bounded by a vertical plate when a strong magnetic field is imposed in a plane that makes various angles with the normal to the plate. The solutions for heat transfer characteristics were evaluated numerically for different parameters such as Prandtl number, magnetic field, suction, visco-elasticity, and the temperature profile. Ishak et al. (2006) carried out a study on unsteady mixed convection boundary layer flow adjacent to a vertical, stretching surface in a viscous and incompressible quiescent fluid. Singh et al. (2007)studied two dimensional free convection and mass transfer flow of an incompressible, viscous and electrically conducting fluid past a continuously moving infinite vertical porous plate in the presence of heat source, thermal diffusion, large suction and uniform magnetic field applied normal to the flow. In the present study the stretching sheet is subjected to a constant injection velocity. The fluid and the stretching sheet are in a state of rigid rotation with a uniform angular velocity about the z-axis. A uniform magnetic field is applied transversely and in a normal direction to the flow. The stretching sheet is considered as a heat source. The resulting finite difference equations are solved numerically by employing a computer program.

2. Flow Analysis and Mathematical Formulation

Consider the unsteady MHD flow of an electrically conducting fluid in a porous medium bounded by two infinite parallel vertical sheets. The sheets are separated by distance H units. Both the fluid and the sheets are in a state of rigid rotation with angular velocity Ω about z-axis normal to the plate. One of the sheets is permeable to allow possible blowing or suction and its surface is subjected to a heat flux q_w. The stretching sheet coincides with the plane $z = 0$ and is stretching at a varying linear velocity of $u = cx$ along the x-axis, where c is the stretching constant

International Electronic Journal of Pure and Applied Mathematics – IEJPAM, Volume 4, No. 4 (2012)

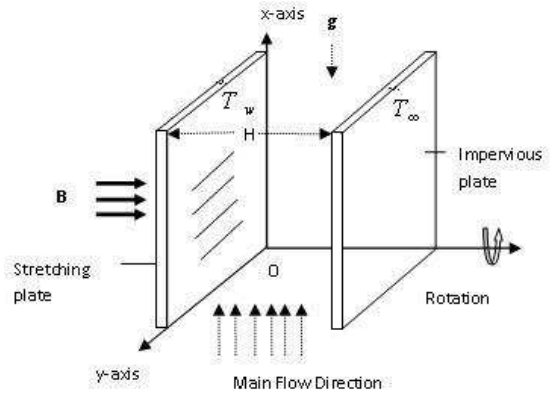

Figure 1: Flow Model

and x is the position along the x-axis. The other sheet is moving at velocity U in the x-axis direction. The x-axis taken to be along the sheet. Stretching takes place upwards against the gravity. The fluid is subjected to a uniform magnetic field $B_o = (0, 0, B_0)$, directed along the positive direction of the z-axis; and there is no external electric field applied. Since both sheets are infinite all physical quantities, except pressure, are functions of z and t. Equation of continuity gives $w = -w_o$, where $w_o > 0$. The equation of conservation of electric change $\nabla \cdot \mathbf{J} = 0$, where $\mathbf{J}$ is the current density, gives $\mathbf{J}_z =$ constant. The current density in component form is $\mathbf{J} = (J_x, J_y, J_z)$. Since the sheets are electrically non-conducting $E = 0$ at the across of the sheets, and thus $J_z = 0$ everywhere in the flow.

Assuming the fluid is weakly ionized, the electron pressure gradient, ion-slip and thermo-electric effects are neglected. Taking Hall current into account, the generalized Ohm's law in absence of electric field is;

$$\mathbf{J} + \frac{\omega_e \tau_e}{H_o} \mathbf{J} \times \mathbf{H} = \sigma(\mathbf{E} + \mu_e \mathbf{q} \times \mathbf{H}) \tag{1}$$

whereω is the electric conductivity, ω_e is the electron frequency, τ_e the electron collision time, $\mathbf{H}$ is the magnetic field vector, μ_e is the magnetic permeability, and $\mathbf{q}$ is

International Electronic Journal of Pure and Applied Mathematics – IEJPAM, Volume 4, No. 4 (2012)

the velocity vector. Mathematically, $B_0 = \mu_e H_0$.

Equation 1 simplifies to;

$$J_x + mJ_y = \sigma\mu_e H_o v \tag{2}$$
$$J_y - mJ_x = -\sigma\mu_e H_o u \tag{3}$$

where $m = \omega_e\tau_e$ is the Hall parameter. On solving equations (2) and (3) for J_x and J_y gives;

$$J_x = \frac{\sigma\mu_e H_o}{1+m^2}(v + mu) \tag{4}$$
$$J_y = \frac{\sigma\mu_e H_o}{1+m^2}(mv - u) \tag{5}$$

The Lorentz force $\mathbf{J} \times \mathbf{B}$ becomes;

$$J_y B_o \mathbf{i} - J_x B_o \mathbf{j} \tag{6}$$

When there is an appreciable difference between the surface and the ambient fluid, one needs to consider the temperature dependent heat source or sink which may exert strong influence on the heat transfer characteristics. Thus temperature dependent volumetric heat generation, and Q is a heat source when $Q > 0$ and is a heat sink when $Q < 0$. Under the usual Boussinesq approximation the equations governing 2-dimensional MHD flow in a rotating system with no imposed pressure gradient are given below.

Equations of momentum:

$$\frac{\partial u}{\partial t} + u\frac{\partial u}{\partial x} - w_o\frac{\partial u}{\partial z} - 2\Omega v = \nu\left(\frac{\partial^2 u}{\partial x^2} + \nu\frac{\partial^2 u}{\partial z^2}\right) - \frac{\nu}{K_p}u + \frac{\sigma B_o^2}{\rho(1+m^2)}(mv - u) + \beta g(T - T_\infty) + \beta^* g(C - C_\infty) \tag{7}$$

where β is volumetric coefficient of thermal expansion, β^* is the volumetric coefficient of thermal expansion due to concentration gradient, σ^* is the Stefan-Boltzmann constant, k^* is the mean absorption coefficient of the fluid, K_p is the Darcy permeability, k_f is thermal conductivity of the porous medium, C_p is the specific heat at constant pressure, D_M is the molecular diffusion coefficient, c_s is the concentration susceptibility, ν is the kinematic viscosity, T_∞ absolute freestream temperature, C_∞ the freestream concentration, g is acceleration due to gravity, and ρ is the density of the fluid.

$$\frac{\partial v}{\partial t} + u\frac{\partial v}{\partial x} - w_o\frac{\partial v}{\partial z} + 2\Omega u = \nu\left(\frac{\partial^2 v}{\partial x^2} + \frac{\partial^2 v}{\partial z^2}\right) - \frac{\nu}{K_p}v - \frac{\sigma B_o^2}{\rho(1+m^2)}(v + mu)$$

International Electronic Journal of Pure and Applied Mathematics – IEJPAM, Volume 4, No. 4 (2012)

(8)

Equation of energy:

$$\begin{aligned}\frac{\partial T}{\partial t}+u\frac{\partial T}{\partial x}-w_o\frac{\partial T}{\partial z} &= \frac{k_f}{\rho C_p}\left(\frac{\partial^2 T}{\partial x^2}+\frac{\partial^2 T}{\partial z^2}\right)+\frac{D_M k_T}{c_s C_p}\left(\frac{\partial^2 C}{\partial z^2}+\frac{\partial^2 C}{\partial x^2}\right)\\ &+ \frac{\sigma}{\rho C_p}B_0^2\left(u^2+v^2\right)+\frac{Q_o}{\rho C_p}(T-T_\infty)\\ &+ \frac{\mu}{\rho C_p}\left[\left(\frac{\partial u}{\partial z}\right)^2+\left(\frac{\partial v}{\partial z}\right)^2\right]-\frac{16\sigma^* T_\infty^3}{3\rho C_p k^*}\frac{\partial^2 T}{\partial z^2}\end{aligned} \tag{9}$$

where Q_o is the temperature dependent volumetric heat generation parameter, σ^* is the Stefan-Boltzmann constant, k^* is the mean absorption coefficient of the fluid, μ is the coefficient of viscosity, T_m is the mean fluid temperature and σ is the electrical conductivity of the fluid.

Equation of Concentration:

$$\frac{\partial C}{\partial t}=D_M\left(\frac{\partial^2 C}{\partial x^2}+\frac{\partial^2 C}{\partial z^2}\right)+\frac{D_M k_T}{T_m}\left(\frac{\partial^2 T}{\partial x^2}+\frac{\partial^2 T}{\partial z^2}\right)-u\frac{\partial C}{\partial x}+w_o\frac{\partial C}{\partial z} \tag{10}$$

Taking the distance between the plates as H units, the physical problem assumes the following initial and boundary conditions.

$$\begin{aligned}t\le 0 &: u=0,v=0,w=0,C=0,T=0 \quad at \quad 0\le z\le H\\ t>0 &: C=C_\infty,T=T_\infty \qquad at \qquad x=0 \quad (Channel \quad entrance)\\ t>0 &: u=cx,v=0,C=C_W,T=T_W,w=w_0 \qquad at \quad z=0 \quad (Porous \quad wall)\\ t>0 &: u=U,v=0,C=C_\infty,T=T_\infty \quad at \quad z=H \quad (Impermeable \quad wall).\end{aligned}$$

The dimensionless parameters are defined as:

$$\begin{aligned}u^{'}=\frac{u}{U},v^{'}=\frac{v}{U},w^{'}=\frac{w}{U},t^{'}=\frac{Ut}{H}\\ y^{'}=\frac{y}{H},x^{'}=\frac{x}{H},z^{'}=\frac{z}{H},T^{'}=\frac{T-T_\infty}{T_W-T_\infty},C^{'}=\frac{C-C_\infty}{C_W-C_\infty}\end{aligned} \tag{11}$$

The non-dimensional form of equations 7 to 10 is;

$$\frac{\partial u^{'}}{\partial t^{'}}-w_o\frac{\partial u^{'}}{\partial z^{'}}-2R_o v^{'}=\frac{1}{Re}\frac{\partial^2 u^{'}}{\partial z^{'2}}-Xiu^{'}-Mu^{'}+\frac{M}{1+m^2}(mv^{'}-u^{'})+Gr_\theta T^{'}+Gr_c C^{'} \tag{12}$$

$$\frac{\partial v^{'}}{\partial t^{'}}-w_o\frac{\partial v^{'}}{\partial z^{'}}+2R_o u^{'}=\frac{1}{Re}\frac{\partial^2 v^{'}}{\partial z^{'2}}-Xiv^{'}-Mv^{'}-\frac{M}{1+m^2}(v^{'}+mu^{'}) \tag{13}$$

International Electronic Journal of Pure and Applied Mathematics – IEJPAM, Volume 4, No. 4 (2012)

$$\frac{\partial T^{'}}{\partial t^{'}} - w_o \frac{\partial T^{'}}{\partial z^{'}} = \frac{1}{PrRe}\frac{\partial^2 T^{'}}{\partial z^{'2}} + D_f Re \frac{\partial^2 C^{'}}{\partial z^{'2}} + \frac{Ec}{Re}\left[\left(\frac{\partial u^{'}}{\partial z^{'}}\right)^2 + \left(\frac{\partial v^{'}}{\partial z^{'}}\right)^2\right] + QT^{'} - \frac{4}{3NPrRe}\left(\frac{\partial^2 T^{'}}{\partial z^{'2}}\right) + RRe\left(u^{'2} + v^{'2}\right) \quad (14)$$

where $Q = \frac{Q_o H}{\rho U C_p}$ is the non-dimensional heat source/sink parameter, Magnetic parameter M, Reynold's number Re, Rotation parameter R_o, Permeability parameter Xi, local temperature Grashof number Gr_θ and local mass Grashof number Gr_c.

$$\frac{\partial C^{'}}{\partial t^{'}} + u^{'}\frac{\partial C^{'}}{\partial x^{'}} - w_o \frac{\partial C^{'}}{\partial z^{'}} = \frac{1}{ReSc}\left(\frac{\partial^2 C^{'}}{\partial x^{'2}} + \frac{\partial^2 C^{'}}{\partial z^{'2}}\right) + \frac{Sr}{Re}\left(\frac{\partial^2 T^{'}}{\partial x^{'2}} + \frac{\partial^2 T^{'}}{\partial z^{'2}}\right) \quad (15)$$

where Sc and Sr is the Schmidt and Soret numbers respectively.

The initial and boundary conditions (11) in dimensionless form translate to;

$$\begin{aligned}
&t^{'} \le 0 \ : \ u^{'} = 0, v^{'} = 0, w^{'} = 0, T^{'} = 0, C^{'} = 0 \quad at \quad 0 \le z^{'} \le H \\
&t^{'} > 0 \ : \ C^{'} = 0, T^{'} = 0 \quad at \quad x^{'} = 0 \ \ (At \ \ Entry) \\
&t^{'} > 0 \ : \ u^{'} = \frac{cH}{U_\infty} x^{'}, v^{'} = 0, C^{'} = 1, T^{'} = 1 \quad at \ \ z^{'} = 0 \ \ (Stretching \ \ sheet) \\
&t^{'} > 0 \ : \ u^{'} = 1, v^{'} = 0, w^{'} = 0, C^{'} = 1, T^{'} = 1 \ \ at \ \ z^{'} = H \ \ (Impermeable \ sheet).
\end{aligned} \quad (16)$$

3. Method of Solution

Equations(12), (13), (14), (15) governing flow in porous media over a stretching surface are coupled and highly non-linear. The approximate numerical solution to the equations is arrived at by employing finite difference method. The equations in their finite difference equivalent form are given below.

Equation of momentum along the x-axis is:

$$\begin{aligned}
U_{i,j}^{k+1} = \ & [U_{i,j}^k - \frac{\Delta T}{2\Delta X}U_{i,j}^k(-U_{i-1,j}^{k+1} + U_{i,j}^k - U_{i-1,j}^k) + \frac{w_o \Delta T}{2\Delta Z}(-U_{i,j-1}^{k+1} + U_{i,j}^k - U_{i,j-1}^k) \\
& + R_o \Delta T(V_{i,j}^{k+1} + V_{i,j}^k) + \frac{\Delta T}{2Re(\Delta X)^2}(U_{i+1,j}^{k+1} + U_{i-1,j}^{k+1} + U_{i+1,j}^k - 2U_{i,j}^k + U_{i-1,j}^k) \\
& + \frac{\Delta T}{2Re(\Delta Z)^2}(U_{i,j+1}^{k+1} + U_{i,j-1}^{k+1} + U_{i,j+1}^k - 2U_{i,j}^k + U_{i,j-1}^k) - \frac{Xi\Delta T}{2}U_{i,j}^k
\end{aligned}$$

International Electronic Journal of Pure and Applied Mathematics – IEJPAM, Volume 4, No. 4 (2012)

$$
\begin{aligned}
& -M\frac{\Delta T}{2}U_{i,j}^{k}+\frac{M\Delta T}{2+2m^{2}}(mV_{i,j}^{k+1}+mV_{i,j}^{k}-U_{i,j}^{k}) \\
+ \quad & \frac{\Delta TGr_{\theta}}{2}(T_{i,j}^{k+1}+T_{i,j}^{k})+\frac{\Delta TGr_{c}}{2}(C_{i,j}^{k+1}+C_{i,j}^{k})]/[1+U_{i,j}^{k}\frac{\Delta T}{2\Delta X} \\
& -\frac{w_{o}\Delta T}{2\Delta Z}+\frac{\Delta T}{Re(\Delta X)^{2}}+\frac{\Delta T}{Re(\Delta Z)^{2}}+\frac{\Delta TXi}{2}+\frac{1}{2}M\Delta T+\frac{M\Delta T}{2+2m^{2}}] \qquad (17)
\end{aligned}
$$

Equation of momentum along the y-axis;

$$
\begin{aligned}
V_{i,j}^{k+1} = \; & [V_{i,j}^{k}-\frac{\Delta T}{2\Delta X}U_{i,j}^{k}(-V_{i-1,j}^{k+1}+V_{i,j}^{k}-V_{i-1,j}^{k})+\frac{w_{o}\Delta T}{2\Delta Z}(-V_{i,j-1}^{k+1}+V_{i,j}^{k}-V_{i,j-1}^{k}) \\
& +R_{o}\Delta T(U_{i,j}^{k+1}+U_{i,j}^{k})+\frac{\Delta T}{2Re(\Delta X)^{2}}(V_{i+1,j}^{k+1}+V_{i-1,j}^{k+1}+V_{i+1,j}^{k}-2V_{i,j}^{k}+V_{i-1,j}^{k}) \\
& +\frac{\Delta T}{2Re(\Delta Z)^{2}}(U_{i,j+1}^{k+1}+V_{i,j-1}^{k+1}+V_{i,j+1}^{k}-2V_{i,j}^{k}+V_{i,j-1}^{k})-\frac{Xi\Delta T}{2}V_{i,j}^{k} \\
& -M\frac{\Delta T}{2}V_{i,j}^{k}+\frac{M\Delta T}{2+2m^{2}}(V_{i,j}^{k}+m(U_{i,j}^{k+1}+U_{i,j}^{k})]/[1+U_{i,j}^{k}\frac{\Delta T}{2\Delta X}-\frac{w_{o}\Delta T}{2\Delta Z} \\
& +\frac{\Delta T}{Re(\Delta X)^{2}}+\frac{\Delta T}{Re(\Delta Z)^{2}}+\frac{Xi\Delta T}{2}+\frac{1}{2}M\Delta T-M\frac{\Delta T}{2+2*m^{2}}] \qquad (18)
\end{aligned}
$$

Equation of energy;

$$
\begin{aligned}
T_{i,j}^{k+1} = \; & [T_{i,j}^{k}+\frac{Q\Delta t}{2}T_{i,j}^{k}-\frac{\Delta t}{2\Delta X}U_{i,j}^{k}(-T_{i-1,j}^{k+1}+T_{i,j}^{k}-T_{i-1,j}^{k}) \\
& +\frac{w_{o}\Delta t}{2\Delta Z}(-T_{i,j-1}^{k+1}+T_{i,j}^{k}-T_{i,j-1}^{k})+\frac{Df\Delta t}{2Re(\Delta X)^{2}}(C_{i+1,j}^{k+1}-2C_{i,j}^{k+1}+C_{i-1,j}^{k+1} \\
& +C_{i+1,j}^{k}-2C_{i,j}^{k}+C_{i-1,j}^{k})+\frac{Df\Delta t}{2Re(\Delta Z)^{2}}(C_{i,j+1}^{k+1} \\
& -2C_{i,j}^{k+1}+C_{i,j-1}^{k+1}+C_{i,j+1}^{k}-2C_{i,j}^{k}+C_{i,j-1}^{k}) \\
& +\frac{Ec\Delta t}{4Re(\Delta X)^{2}}(U(i,j,k+1)-U_{i-1,j}^{k+1}+U_{i,j}^{k}-U_{i-1,j}^{k})^{2} \\
& +\frac{Ec\Delta t}{4Re(\Delta Z)^{2}}(U(i,j,k+1)-U_{i,j-1}^{k+1}+U_{i,j}^{k} \\
& -U_{i,j-1}^{k})^{2}]/[1+\frac{\Delta T}{2\Delta X}U_{i,j}^{k}-\frac{w_{o}\Delta t}{2\Delta Z} \\
& +\frac{\Delta t}{RePr(\Delta X)^{2}}+\frac{\Delta t}{RePr(\Delta Z)^{2}} \\
& -\frac{Q\Delta t}{2}-\frac{4\Delta t}{3NiPrRe(\Delta Z)^{2}}]
\end{aligned}
\qquad (19)
$$

Equation of concentration;

$$
C_{i,j}^{k+1} = [C_{i,j}^{k}-\frac{\Delta t}{2\Delta X}U_{i,j}^{k}(-C_{i-1,j}^{k+1}+C_{i,j}^{k}-C_{i-1,j}^{k})+\frac{w_{o}\Delta t}{2\Delta Z}(-C_{i,j-1}^{k+1}+C_{i,j}^{k}-C_{i,j-1}^{k})
$$

International Electronic Journal of Pure and Applied Mathematics – IEJPAM, Volume 4, No. 4 (2012)

$$+\frac{\Delta t}{2ScRe(\Delta X)^2}(C^{k+1}_{i+1,j}+C^{k+1}_{i-1,j}+C^{k}_{i+1,j}-2C^{k}_{i,j}+C^{k}_{i-1,j})$$
$$+\frac{\Delta t}{2ScRe(\Delta Z)^2}(C^{k+1}_{i,j+1}+C^{k+1}_{i,j-1}+C^{k}_{i,j+1}-2C^{k}_{i,j}+C^{k}_{i,j-1})$$
$$+\frac{Sr\Delta t}{2Re(\Delta X)^2}(T^{k+1}_{i+1,j}-2T^{k+1}_{i,j}+T^{k+1}_{i-1,j}$$
$$+T^{k}_{i+1,j}-2T^{k}_{i,j}+T^{k}_{i-1,j})+\frac{Sr\Delta t}{2Re(\Delta Z)^2}(T^{k+1}_{i,j+1}-2T^{k+1}_{i,j}$$
$$+T^{k+1}_{i,j-1}+T^{k}_{i,j+1}-2T^{k}_{i,j}+T^{k}_{i,j-1})]/[1+\frac{\Delta t}{2\Delta X}U^{k}_{i,j}$$
$$-\frac{w_o\Delta t}{2\Delta Z}+\frac{\Delta t}{ReSc(\Delta X)^2}+\frac{\Delta t}{ReSc(\Delta Z)^2}] \tag{20}$$

The variables $u^{'}$, $v^{'}$, $C^{'}$,and $T^{'}$ are represented by the variables U, V, C, and T respectively in the finite difference equations. The values of U in equation (17)are determined at every nodal point for a particular i at $(k+1)^{th}$ time level. Similarly, the values of V are calculated from equation (18). Using the values of U and V at $(k+1)^{th}$ time level, the values of C at $(k+1)^{th}$ time level in equation (20) are found in a similar manner. Thus, the values of U, V and C are known on a particular i-level. Finally the values of T are calculated using equation (19) at every nodal point on a particular i-level at $(k+1)^{th}$ time level at every nodal point on a particular i-level at $(k+1)^{th}$ time level. This process is repeated for various i-levels. Thus the values of U, V, C and T are determined at all grid points in the rectangular region at $(k+1)^{th}$ time level. The mesh sizes are taken as $\Delta X = 0.05$, $\Delta Z = 0.25$, and $\Delta t = 0.001$. It is observed that, when mesh size is reduced the results do not have a significant difference. Hence, the above mentioned sizes have been considered as appropriate mesh sizes for calculation. The local truncation error is $O(\Delta t + (\Delta Z)^2 + (\Delta X)^2)$ and it tends to zero as Δt, ΔZ , and ΔX tend to zero. Thus the present employed scheme is convergent.

4. Local Nusselt Number, Sherwood Number, and Shearing Stress

In technological applications, the local Nusselt number, the local Sherwood number, and the shearing stress on the stretching sheet are of primary interest.

The local skin friction coefficients are defined as;

$$C_{fx} = -\frac{\tau_x}{\frac{1}{2}\rho U^2} = -\frac{2}{Re}\left(\frac{\partial u'}{\partial z'}\right)_{z'=0} \tag{21}$$

$$C_{fy} = -\frac{\tau_x}{\frac{1}{2}\rho U^2} = -\frac{2}{Re}\left(\frac{\partial v'}{\partial z'}\right)_{z'=0} \tag{22}$$

International Electronic Journal of Pure and Applied Mathematics – IEJPAM, Volume 4, No. 4 (2012)

Equations (21) and (22) represent the respective local skin friction coefficients due to primary and secondary velocity profiles. For some suitable length H along the stretching sheet, Sherwood number (Sh)is given by;

$$Sh = \frac{Q_w}{C_W - C_\infty} \cdot \frac{H}{D_M} = -\left(\frac{\partial C'}{\partial z'}\right)_{z'=0} \tag{23}$$

$$q_w = -k_f \frac{\partial T}{\partial z} \tag{24}$$

where k_f is the thermal conductivity of the saturated porous medium. The local Nusselt number (Nu) is given as

$$\begin{aligned} Nu &= \frac{q_w}{T_W - T_\infty} \cdot \frac{H}{k_f} \\ &= \left(\frac{\partial T'}{\partial z'}\right)_{z'=0} \end{aligned} \tag{25}$$

Using the method of Least Squares, the following approximating quadratic bivariate polynomial is used; $P_i(z,t) = a_1 + b_1 z + c_1 t + d_1 z^2 + e_1 t^2 + f_1 zt$.

To obtain an approximating bivariate polynomial for $U(z,t)$, the following equation is minimized:

$$I(a_1, b_1, c_1, d_1, e_1, f_1) = \sum_{i=1}^{n} \left[U(z_i, t_i) - (a_1 + b_1 z_i + c_1 t_i + d_1 z_i^2 + e_1 t_i^2 + f_1 z_i t_i)\right]^2 \tag{26}$$

where n is the number of point used, and z and t represent distance along z-axis and time respectively. Taking 9 nodal points in the discretised flow domain, the values of t, z, and U are taken as given in Table 1.

Table 1: Values of t, z and U(z,t) for M = 1, Pr = 0.71, m = 0.5, N = 0.45, Q = 0.8, R = 0.2, Ec = 0.4, Sc = 0.78, Xi = 0.5, Sr = 1, Ro = 0.3, w_o = -0.5, Re = 50, Df = 0.03, $Gr_\theta = 5$, $Gr_c = 2$.

t	0.399	0.400	0.401	0.402	0.403	0.404
z	0	0.03	0.06	0.09	0.12	0.15
U(z,t)	0.36538	0.42951	0.44124	0.44298	0.44328	0.44340

t	0.407	0.408	0.409
z	1.75	2.00	2.25
U(z,t)	0.44349	0.44359	0.44368

Using the values given in Table 1, the matrix A of coefficients $a_1, b_1, c_1, d_1, e_1, f_1$

International Electronic Journal of Pure and Applied Mathematics – IEJPAM, Volume 4, No. 4 (2012)

becomes;

$$A = \begin{pmatrix} 10 & 1.08 & 3.627 & 0.1836 & 1.461741 & 0.43704 \\ 1.08 & 0.1836 & 0.43704 & 0.03499 & 0.17686 & 0.07442 \\ 3.627 & 0.43704 & 1.46174 & 0.07442 & 0.58913 & 0.17686 \\ 0.1836 & 0.03499 & 0.07442 & 0.00711 & 0.03017 & 0.01419 \\ 1.46174 & 0.17686 & 0.58913 & 0.03017 & 0.23745 & 0.07157 \\ 0.43704 & 0.07442 & 0.17686 & 0.01419 & 0.07157 & 0.03017 \end{pmatrix} \tag{27}$$

The column matrix given by the left-hand side of equation 26 is given as matrix C shown below;

$$C = \begin{pmatrix} 3.89653876 \\ 0.478395677 \\ 1.570665488 \\ 0.081410076 \\ 0.633148648 \\ 0.193593544 \end{pmatrix} \tag{28}$$

The column matrix of the constants $a_1, b_1, \cdots, f_1$ is given by matrix B shown below.

$$B = \begin{pmatrix} a_1 \\ b_1 \\ c_1 \\ d_1 \\ e_1 \\ f_1 \end{pmatrix} \tag{29}$$

The matrix equation **AB=C** is solved using Matlab command $B = A\backslash C$ so as to obtain the constants $a_1, b_1, \cdots, f_1$. These constants are used in evaluating the four bivariates shown below:

$U(z,t) = 0.7176z + 1.9392t - 2.7097335z^2 - 2.434t^2 + 0.3284zt.$

Similarly the bivariates for $V(z,t)$, $C(z,t)$ and $T(z,t)$ are:

$V(z,t) = -0.1017z - 0.2544t + 0.2402z^2 + 0.4897t^2 + 0.0523zt.$

$C(z,t) = -0.5891z - 0.7827t + 3.7904z^2 + 3.0699t^2 - 1.5768zt.$

$T(z,t) = 0.6348z + 0.7132t + 0.5181z^2 + 0.8454t^2 - 1.7645zt.$

The bivariates for U, V, C and T obtained above are used in obtaining the results shown in Table 2.

5. Results and Discussion

In order to get a physical insight into the problem at hand, the velocity, temperature and concentration fields have been discussed by assigning numerical values to various

International Electronic Journal of Pure and Applied Mathematics – IEJPAM, Volume 4, No. 4 (2012)

Table 2: Variation of Coefficients of friction, Sherwood and Nusselt numbers with various parameters.

M	Pr	m	N	Q	R	Ec	t	C_{fx}	C_{fy}	Sh	Nu
1.0	0.71	0.50	0.45	0.8	0.2	0.40	0.4	-0.03396	0.00323	1.21982	0.07100
2.0	0.71	0.50	0.45	0.8	0.2	0.40	0.4	-0.02207	0.00212	1.25290	0.16228
3.0	0.71	0.50	0.45	0.8	0.2	0.40	0.4	-0.01369	0.00206	1.25974	0.26508
1.0	0.89	0.50	0.45	0.8	0.2	0.40	0.4	-0.03398	0.00335	1.19728	0.09954
1.0	0.64	0.50	0.45	0.8	0.2	0.40	0.4	-0.03322	0.00329	1.23594	0.04404
1.0	0.71	1.00	0.45	0.8	0.2	0.40	0.4	-0.03735	0.00258	1.20272	0.03108
1.0	0.71	1.50	0.45	0.8	0.2	0.40	0.4	-0.03887	0.00144	1.19998	0.01416
1.0	0.71	0.50	0.10	0.8	0.2	0.40	0.4	-0.04531	0.00353	1.55106	-1.56942
1.0	0.71	0.50	1.00	0.8	0.2	0.40	0.4	-0.03169	0.00310	1.15656	0.31710
1.0	0.71	0.50	0.45	1.4	0.2	0.40	0.4	-0.03443	0.00316	1.21932	0.04528
1.0	0.71	0.50	0.45	2.0	0.2	0.40	0.4	-0.03490	0.00310	1.21882	0.03022
1.0	0.71	0.50	0.45	0.8	0.5	0.40	0.4	-0.03651	0.00371	1.23336	-0.22190
1.0	0.71	0.50	0.45	0.8	1.5	0.40	0.4	-0.04626	0.00382	1.27518	-1.41616
1.0	0.71	0.50	0.45	0.8	0.2	0.80	0.4	-0.03378	0.00328	1.21288	0.06726
1.0	0.71	0.50	0.45	0.8	0.2	1.00	0.4	-0.03360	0.00340	1.20916	0.06352
1.0	0.71	0.50	0.45	0.8	0.2	0.40	0.6	-0.03459	0.00313	1.21526	0.04784
1.0	0.71	0.50	0.45	0.8	0.2	0.40	0.8	-0.03472	0.00247	1.21262	0.04078

non-dimensional parameters. For instance the following parameters have been used: M = 1, Pr = 0.71, m = 0.5, N = 0.45, Q = 0.8, R = 0.2, Ec = 0.4, Sc = 0.78, Xi = 0.5, Sr = 1, Ro = 0.3, w_o = -0.5, Re = 50, Df = 0.03, $Gr_\theta = 5$, and $Gr_c = 2$. The values of Prandtl number Pr used are 0.64, 0.71, and 7.00 and represent flue gas, air, and water respectively at 20^oC and one atmosphere pressure. The values of Schmidt number used are 0.22, 0.62, and 0.78 and represent hydrogen, water vapour and ammonia respectively at 20^oC and one atmosphere pressure. A positive value of thermal Grashof number ($Gr_\theta > 0$) corresponds to a cooled sheet.

Figure 2 and Figure 3 show that in the presence of a heat source, increase in Hall parameter m leads to an increase in the magnitude of primary velocity profiles and secondary velocity profiles respectively. Increase in Magnetic parameter M leads to a decrease in the magnitude of primary velocity profiles and secondary velocity profiles respectively. A large value of M causes a reversal in the direction of the secondary velocity profiles. The fluid velocity increases with increasing m due to the fact that the effective conductivity of the fluid decreases with increase in the Hall parameter m, since the magnetic damping force is reduced. However the magnetic damping force increases with increasing M, causing a decrease in the velocity profiles. Increase in time t leads to an increase in the magnitude of the primary and secondary velocity profiles respectively.

Figure 4 shows that an increase in Hall parameter m leads to a decrease in the concentration profiles. An increase in the Magnetic parameter M leads to an

International Electronic Journal of Pure and Applied Mathematics – IEJPAM, Volume 4, No. 4 (2012)

increase in the concentration profiles. Increase in m leads to decrease in the conductivity of the fluid, reducing the magnetic damping force. This increases the rate of transportation of the species by convection away from the boundary layer region, leading to lower species concentration. Similarly, increase in M leads to an increase in the magnetic damping force, resulting to an increase in the concentration profiles. Increase in the concentration profiles is as a result of reduced rate of species transportation. Increase in time t leads to a decrease in the concentration profiles. Thus concentration of the fluid decreases with time.

From Figure 5 increase in the Hall parameter m causes increase in the temperature profiles. Increasing m decreases the conductivity of the fluid, resulting in increase in Joule heating, leading to a thicker thermal boundary layer. Increase in the Magnetic parameter M leads to a decrease in the temperature profiles. Reduced velocity implies lower viscous dissipation and hence the observed decrease in the temperature profiles.

Figures 6, 7, 8 and 9 show that in the presence of a heat source ($Q > 0$), increase in the Schmidt number Sc causes a decrease in the velocity profiles. Increase in Sc causes an increase in concentration and temperature profiles respectively. Physically increase in concentration implies that when subjected to a heat source, Hydrogen diffuses faster in Air (Pr=0.71) than Water vapour does; and Water vapour diffuses slower in Air than it does in Ammonia. Increase in temperature implies that under similar conditions, a mixture of Air and Hydrogen is warmer than a mixture of Air and Water vapour; and Water vapour is warmer than a mixture of Air and Ammonia. Increase in concentration with increase in Sc shows that Ammonia diffuses faster into Air than it does in Water vapour and Hydrogen respectively. A large value of Sc implies a heavier fluid. Figure 9 shows that there is a cross-over of the temperature profiles at along the stretching sheet. A cross-over in the temperature profiles takes place when the effects of stretching on temperature is overcome by the effects of Schmidt number on the temperature in the thermal boundary layer region. Increase in time t leads to a decrease in the velocity, temperature and concentration profiles of the fluid.

Figures 6, 7, 8 and 9 show that in the presence of a heat source ($Q > 0$), increase in Prandtl number Pr causes an increase in the velocity and concentration profiles respectively. Increase in Pr causes a decrease in temperature profiles. Physically this means that when subjected to similar conditions, a mixture of Flue gas (Pr = 0.64) and Hydrogen (Sc = 0.22, at 25^oC temperature and one atmosphere pressure) diffuses faster than does a mixture of Air and Hydrogen; and a mixture of Air and Hydrogen diffuses faster than a mixture of Water and Hydrogen. Under similar conditions, Hydrogen diffuses faster in Flue gas than it does in the Air; and the latter diffuses less faster in Water. Increase in time t causes a decrease in concentration and temperature profiles respectively. Increase in time causes an increase in velocity profiles.

Figures 10, 11, 12 and 13 show that increase in the magnitude of the Heat

International Electronic Journal of Pure and Applied Mathematics – IEJPAM, Volume 4, No. 4 (2012)

sink parameter Q leads to a decrease in the magnitude of velocity and temperature profiles respectively. Increase in Q leads to an increase in the concentration profiles. The presence of a heat sink produces a cooling effect that decreases velocity of the convection currents that move upwards next to the surface of the stretching sheet, leading to higher concentration profiles.

Figures 10, 11, 12 and 13 show that in the presence of a heat sink, increase in the Eckert number Ec leads to an increase in the magnitude of the velocity and temperature profiles respectively; but to a decrease in the concentration profiles. Increase in Ec means the fluid absorbs more heat energy that is released from the internal viscous forces. This in turn increases the temperature and the velocity of the convection currents due to increased thermal buoyancy forces respectively. Higher velocity profiles implies an increased rate of species transportation away from the boundary layer region, and hence the observed decrease in the concentration profiles.

Figures 10, 11, 12 and 13 show that in the presence of a heat sink, increase in the Radiation parameter N leads to a decrease in the magnitude of the velocity and temperature profiles respectively; but to an increase in the concentration profiles. Thus radiation can be used to control the velocity and thermal boundary layers quite effectively. Increase in time t leads to an increase in the magnitude of the velocity, concentration and temperature profiles. This shows that the transient velocity, concentration and temperature increase with time.

Figures 14, 15, 16 and 17 show that in the presence of a heat sink, increase in the magnitude of the Injection parameter w_o leads to an increase in the velocity and temperature profiles respectively; but to a decrease in the concentration profiles. Injection increases the velocity of the fluid thus increasing the rate at which the species are carried away from the boundary layer region, and hence the observed decrease in the species concentration. Thus velocity, temperature and concentration boundary layers can be controlled by varying the rate of injection. Increase in the Permeability parameter Xi leads to a decrease in the velocity and temperature profiles; but to an increase in the concentration profiles. Increase in the Rotation parameter Ro leads to a decrease in the velocity and temperature profiles; but to an increase in the concentration profiles. Increase in Xi will results in increased resistance to the flow by the porous medium (as the permeability physically becomes less with increasing Xi) which will in turn lead to deceleration of the flow velocity of the fluid; resulting into reduced magnitudes of the primary and the secondary velocities respectively. Increase in the Joule heating parameter R leads to an increase in the velocity and temperature profiles respectively; but to a decrease in the concentration profiles. Increase in Joule heating parameter leads to the heating of the fluid thereby boosting the velocity of the convection currents on the surface of the stretching sheet.

From Table 2 the following observations are noted:

1. When $Q > 0$, increase in the Magnetic parameter M leads to a decrease in the magnitude of the local skin-friction coefficients C_{fx} and C_{fy} due to the

International Electronic Journal of Pure and Applied Mathematics – IEJPAM, Volume 4, No. 4 (2012)

primary and the the secondary velocity profiles respectively. The decreasing frictional drag is due to increase in the Lorentz force that decreases the primary velocity of the fluid. Decrease in C_{fy} is due to decreasing secondary velocity with increasing M. Increase in M leads to an increase in the Sherwood number Sh and in Nusselt number Nu respectively. Increase in M leads to increase in the concentration gradients hence the observed increase in the value of Sh. Increase in the value of M results into a lower rate of transportation of the species in the concentration boundary layer. Thermal boundary layer thickness decreases with increase in M leading to the observed increase in the Nusselt number.

2. When $Q > 0$ increase in the Prandtl number Pr leads to an increase in the magnitude of C_{fx} and C_{fy} respectively; but to a decrease in Sh and Nu respectively. Increase in Pr leads to higher velocities and hence the observed increase in the values C_{fx} and C_{fy} respectively. Fluids which are good conductors of heat have a relatively small value of Prandtl number. Increase Pr decreases the thickness of thermal boundary layer leading to a higher rate of heat transfer. Decrease in Sherwood number is due to an increased rate of transportation of the species toward the the surface of the stretching sheet due to increased velocity of the fluid.

3. When $Q > 0$ increase in the Hall parameter m leads to an increase in the magnitude of C_{fx}, Sh and Nu respectively; but to a decrease in C_{fy}. Increase in m leads to higher primary velocity thereby increasing the shear stress C_{fx}. Decrease in the magnitude of the secondary velocity profiles lead to a decrease in C_{fy}. Increase in m increases the Joule heating since the conductivity of the fluid decreases, leading to a thicker thermal boundary layer. This leads to a reduced rate of heat transfer.

4. Increase in the Radiation parameter N leads to an increase in the magnitudes of C_{fx}, C_{fy}, and Nu respectively; but to a decrease in Sh. Increase in N leads to an increase in the rate of species transportation. This result qualitatively agrees with expectations, since the effect of radiation is to decrease the rate of energy transport to the fluid, thereby decreasing the temperature of the fluid. Increase in Radiation parameter leads to a thinner thermal boundary layer, leading to an increase in the rate of heat transfer. Increase in N enhances convection currents on the surface of the sheet, leading to increase in C_{fx} and C_{fy} respectively.

5. Increase in the heat source parameter Q leads to an increase in the magnitudes of C_{fx}, C_{fy} respectively; but to a decrease in the Sherwood number Sh and Nusselt number Nu respectively. Increase in Q enhances convection currents on the surface of the sheet, leading to increase in C_{fx} and C_{fy} respectively.

Increase in Q leads to a thicker thermal boundary layer, leading to lower temperature gradients leading to a decrease in Nu.

6. Increase in the Joule heating parameter R leads to an increase in C_{fx}, C_{fy}, Sh and Nu respectively. The results qualitatively agree with what is expected since the effect of Joule heating is to decrease the rate of energy transport to the fluid, thereby decreasing the temperature of the fluid. Increase in the velocity of the fluid leads to an increase in the values of C_{fx} and C_{fy}, that in turn lead to a decrease in the species concentration.

7. Increase in the Eckert number Ec leads to an increase in C_{fx}, C_{fy} but to a decrease in Nu and Sh respectively. Increasing the velocity of the fluid leads to an increase in the species concentration. A positive Eckert number implies cooling of the stretching sheet thereby enhancing convection currents leading to increased velocity and the temperature of the fluid respectively. The resulting thicker thermal boundary layer leads to a reduced rate of heat transfer.

8. Increase in time t leads to a decrease in the magnitude of C_{fx}, C_{fy}, Nu and Sh respectively. This physically means that shear stresses C_{fx} and C_{fy}, Nu and Sh decrease with time. This is expected since the velocity, temperature and concentration of the fluid decrease gradually with time, finally equalising with their respective freestream values.

Acknowledgments

We are grateful to JKUAT Training Committee for financial help in preparation of this paper.

References

[1] A. Ishak, R. Nazar, Unsteady mixed convection boundary layer flow due to a stretching vertical surface, *The Arabian Journal for Science and Engineering*, **31**, No. 2B (2006).

[2] M. Kinyanjui, N. Chaturvedi, S.M. Uppal, MHD Stokes problem for a vertical infinite plate in a dissipative rotating fluid with Hall current, *Energy Conversion and Management*, **39** (1998), 541-548.

[3] M. Kinyanjui, J.K. Kwanza, S.M. Uppal, MHD free convection heat and mass transfer of a heat generating fluid past an impulsively started infinite vertical porous plate with Hall current and radiation absorption, *Energy Conversion and Management*, **42** (2001), 917-931.

[4] P.C. Ram, Hall effects on hydromagnetic convective flow in a rotating fluid through porous medium, *Journal of Engineering Science*, **5**, No. 1 (1991), 43-53.

[5] Singh, Atul Kumar, Numerical solution of hydromagnetic unsteady unsteady free convection flow past an infinite porous plate, *Indian Journal of Pure and Applied Physics*, **41** (2003), 167-70.

[6] M. Subhas, A. Joshi, R.M. Sonth, Heat transfer in MHD visco-elastic fluid flow over a stretching surface, *ZAMM – Z. Angew. Math. Mech.* **81** (2001), No. 10, 691-698.

International Electronic Journal of Pure and Applied Mathematics – IEJPAM, Volume 4, No. 4 (2012)

International Electronic Journal of Pure and Applied Mathematics – IEJPAM, Volume 4, No. 4 (2012)

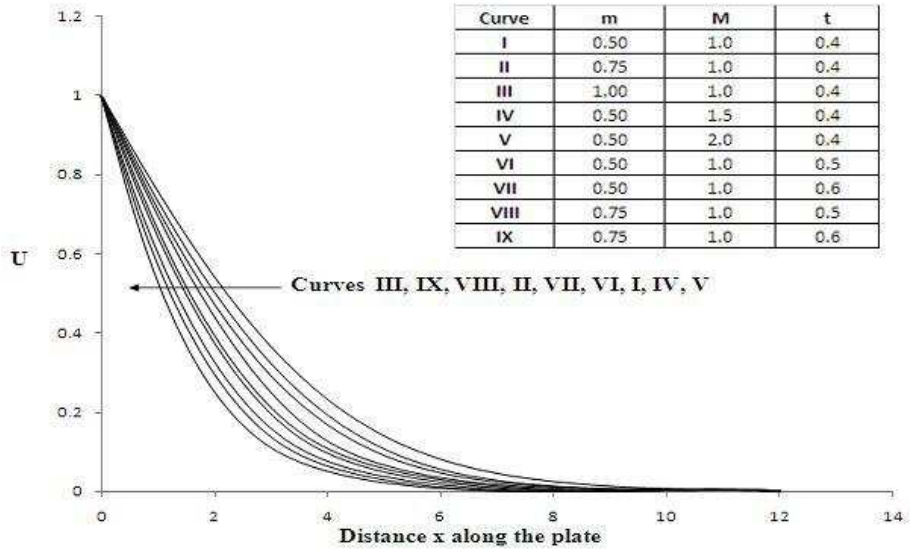

Figure 2: Primary velocity profiles when m, M and t are varied.

International Electronic Journal of Pure and Applied Mathematics – IEJPAM, Volume 4, No. 4 (2012)

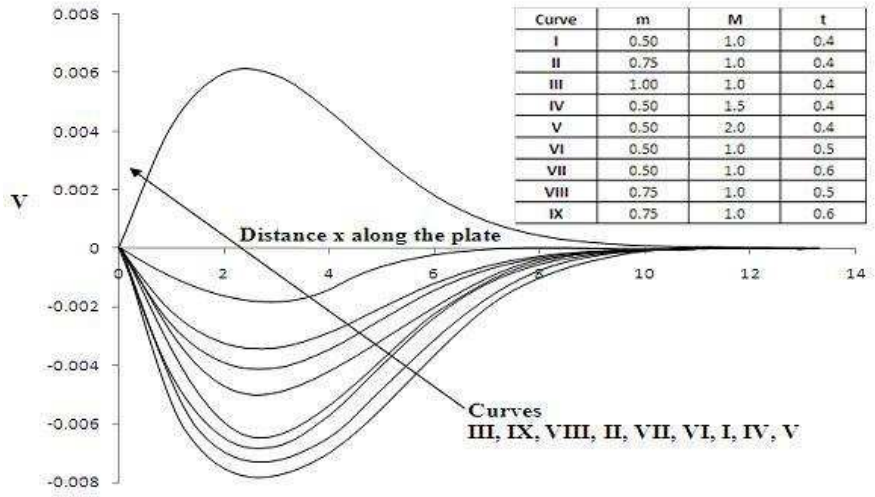

Curve	m	M	t
I	0.50	1.0	0.4
II	0.75	1.0	0.4
III	1.00	1.0	0.4
IV	0.50	1.5	0.4
V	0.50	2.0	0.4
VI	0.50	1.0	0.5
VII	0.50	1.0	0.6
VIII	0.75	1.0	0.5
IX	0.75	1.0	0.6

Figure 3: Secondary velocity profiles when m, M and t are varied.

International Electronic Journal of Pure and Applied Mathematics – IEJPAM, Volume 4, No. 4 (2012)

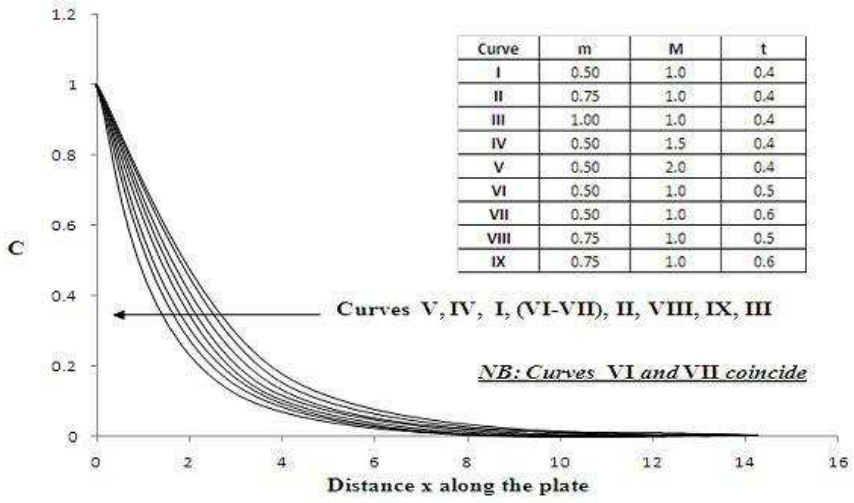

Figure 4: Concentration profiles when m, M and t are varied.

International Electronic Journal of Pure and Applied Mathematics – IEJPAM, Volume 4, No. 4 (2012)

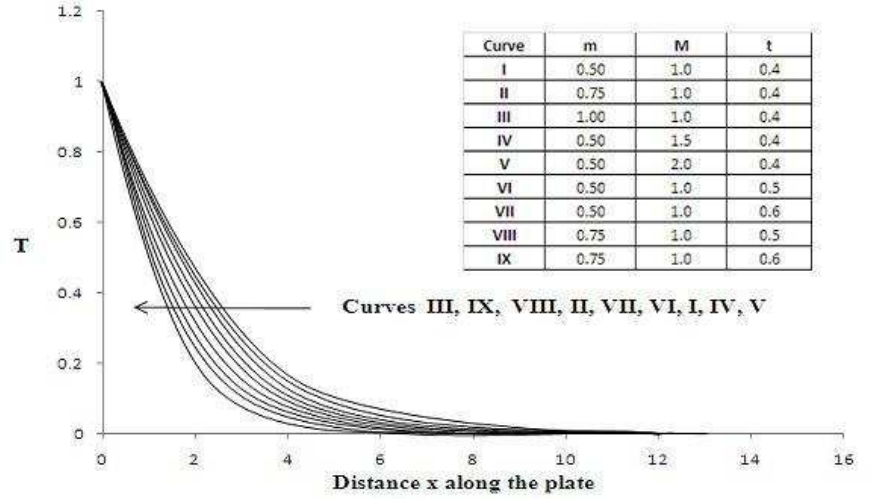

Figure 5: Temperature profiles when m, M and t are varied.

International Electronic Journal of Pure and Applied Mathematics – IEJPAM, Volume 4, No. 4 (2012)

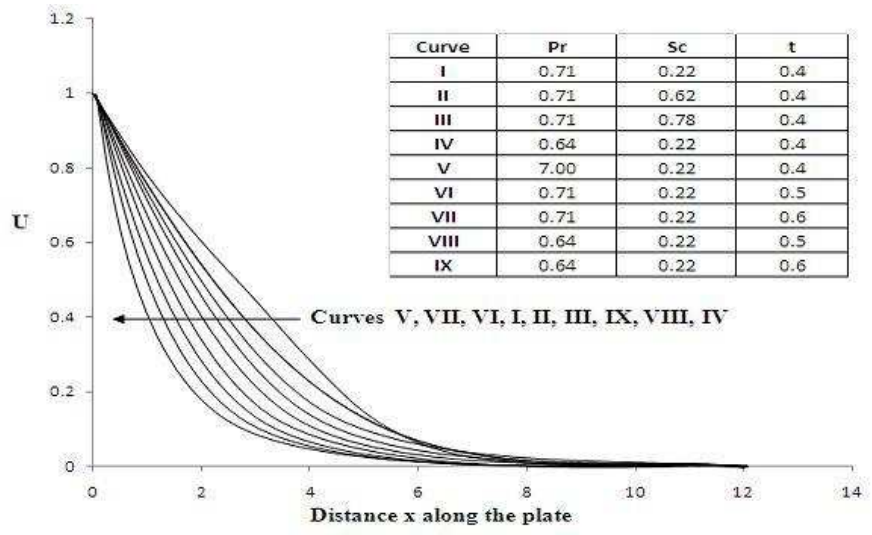

Figure 6: Primary velocity profiles when Pr, Sc and t are varied.

International Electronic Journal of Pure and Applied Mathematics – IEJPAM, Volume 4, No. 4 (2012)

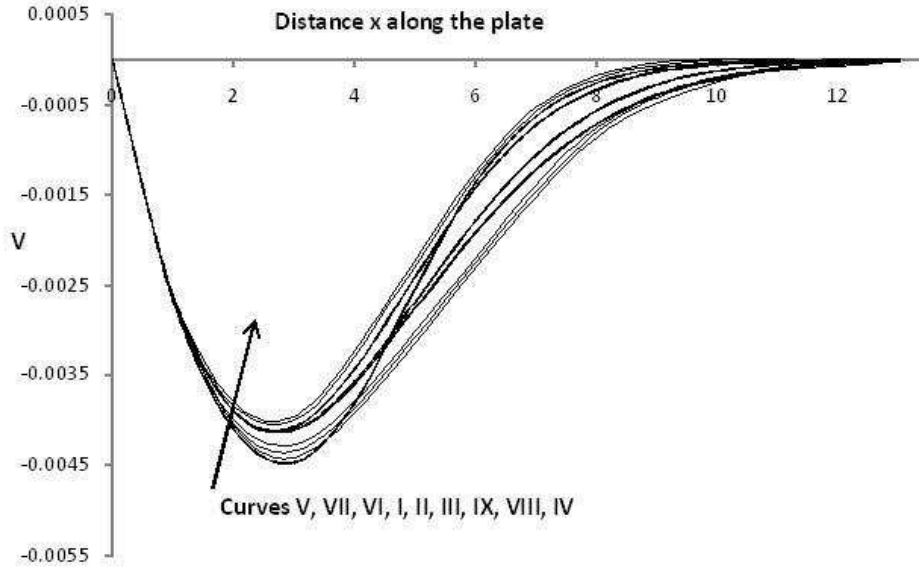

Figure 7: Secondary velocity profiles when Pr, Sc and t are varied.

International Electronic Journal of Pure and Applied Mathematics – IEJPAM, Volume 4, No. 4 (2012)

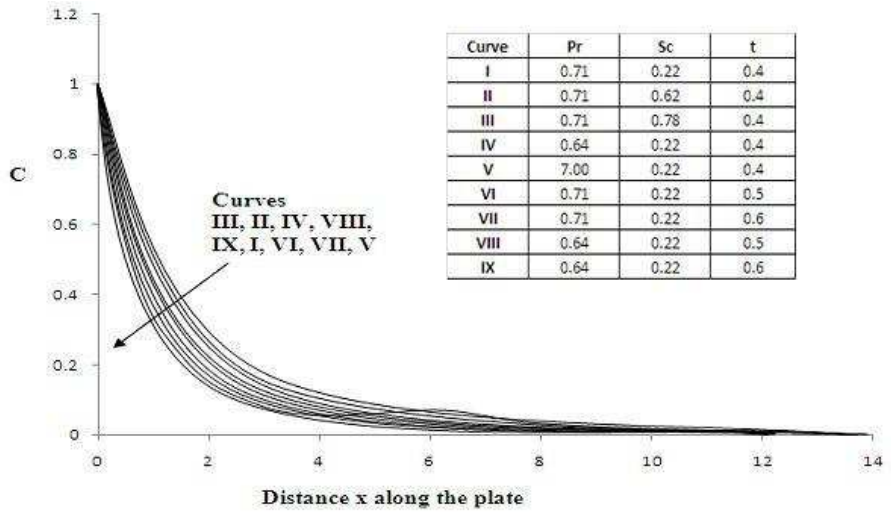

Curve	Pr	Sc	t
I	0.71	0.22	0.4
II	0.71	0.62	0.4
III	0.71	0.78	0.4
IV	0.64	0.22	0.4
V	7.00	0.22	0.4
VI	0.71	0.22	0.5
VII	0.71	0.22	0.6
VIII	0.64	0.22	0.5
IX	0.64	0.22	0.6

Figure 8: Concentration profiles when Pr, Sc and t are varied.

International Electronic Journal of Pure and Applied Mathematics – IEJPAM, Volume 4, No. 4 (2012)

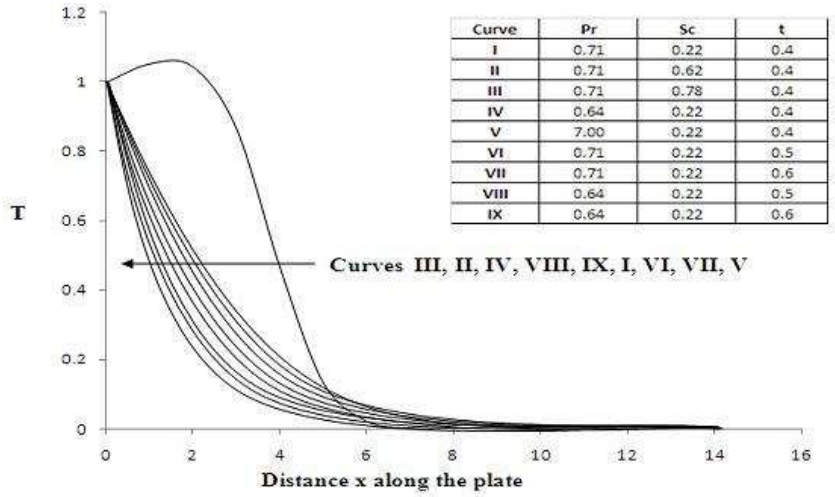

Figure 9: Temperature profiles when Pr, Sc and t are varied.

International Electronic Journal of Pure and Applied Mathematics – IEJPAM, Volume 4, No. 4 (2012)

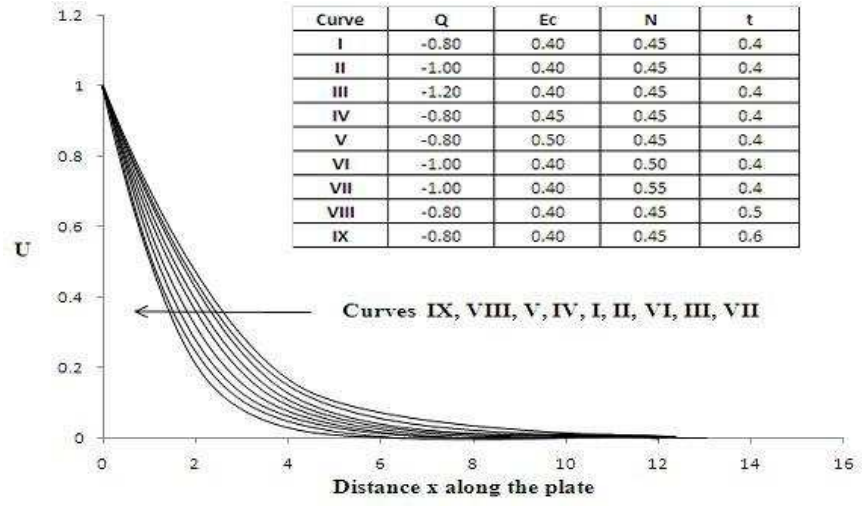

Figure 10: Primary velocity profiles when Q, Ec, N, and t are varied.

International Electronic Journal of Pure and Applied Mathematics – IEJPAM, Volume 4, No. 4 (2012)

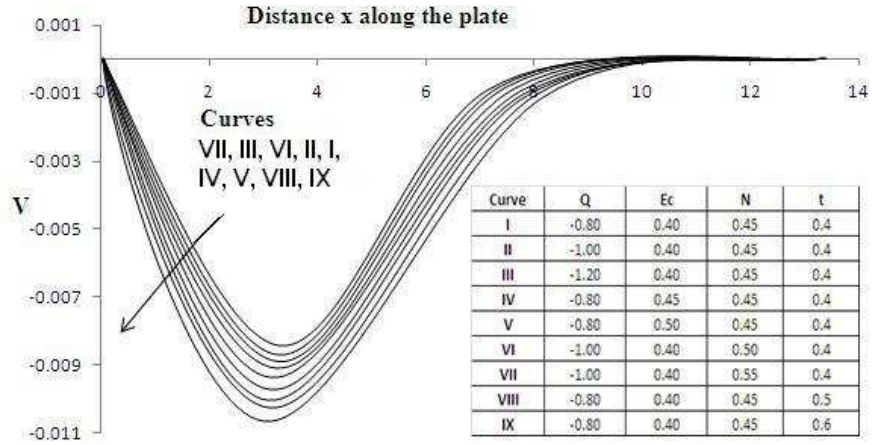

Curve	Q	Ec	N	t
I	-0.80	0.40	0.45	0.4
II	-1.00	0.40	0.45	0.4
III	-1.20	0.40	0.45	0.4
IV	-0.80	0.45	0.45	0.4
V	-0.80	0.50	0.45	0.4
VI	-1.00	0.40	0.50	0.4
VII	-1.00	0.40	0.55	0.4
VIII	-0.80	0.40	0.45	0.5
IX	-0.80	0.40	0.45	0.6

Figure 11: Secondary velocity profiles when Q, Ec, N, and t are varied.

International Electronic Journal of Pure and Applied Mathematics – IEJPAM, Volume 4, No. 4 (2012)

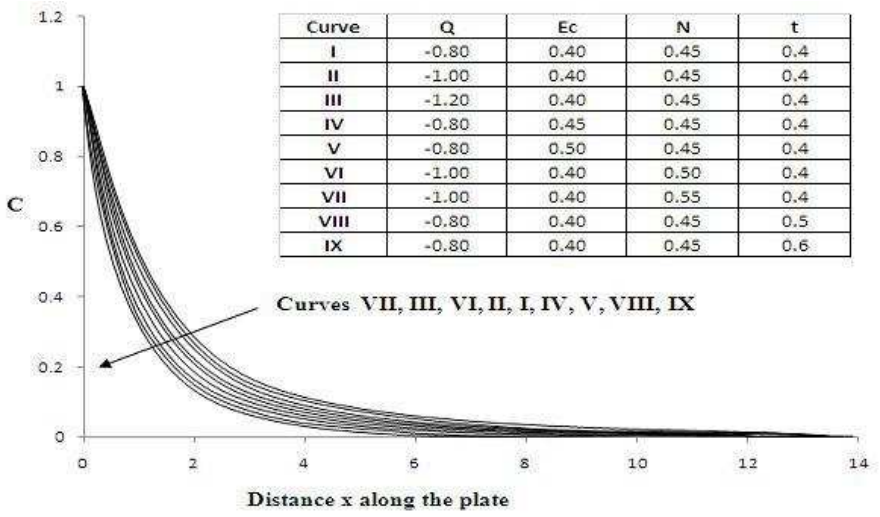

Figure 12: Concentration profiles when Q, Ec, N, and t are varied.

International Electronic Journal of Pure and Applied Mathematics – IEJPAM, Volume 4, No. 4 (2012)

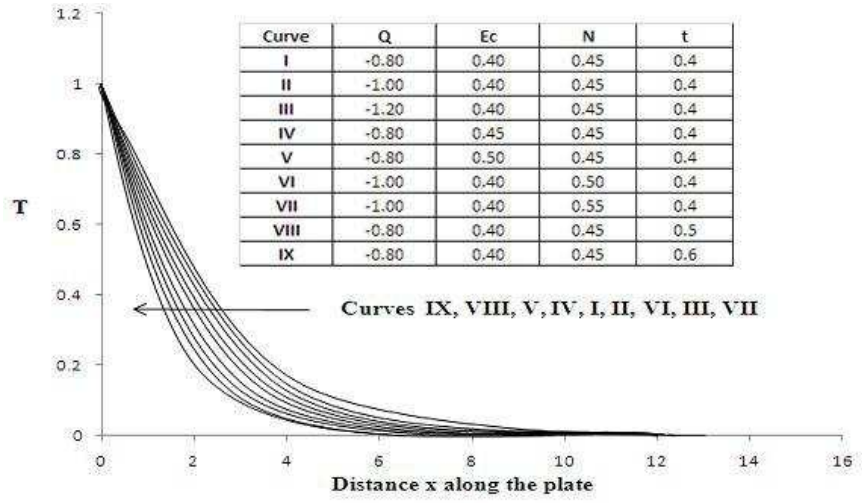

Figure 13: Temperature profiles when Q, Ec, N, and t are varied.

International Electronic Journal of Pure and Applied Mathematics – IEJPAM, Volume 4, No. 4 (2012)

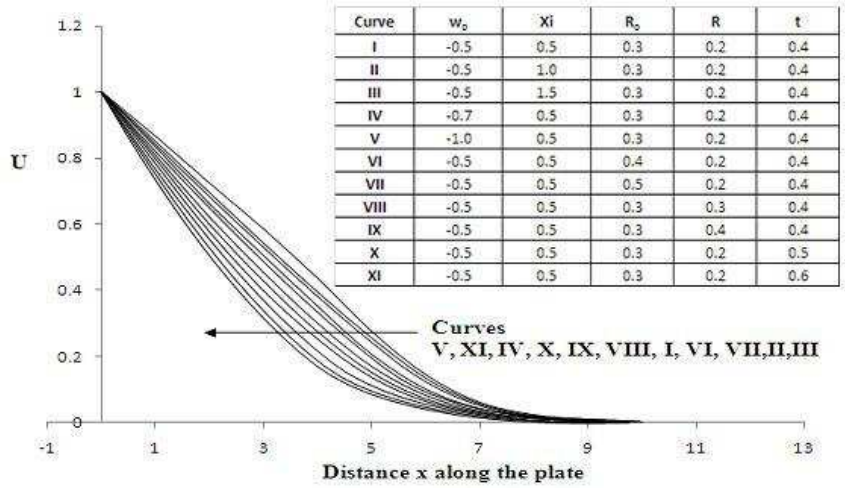

Figure 14: Primary velocity profiles when w_o, Xi, Ro, R, and t are varied.

International Electronic Journal of Pure and Applied Mathematics – IEJPAM, Volume 4, No. 4 (2012)

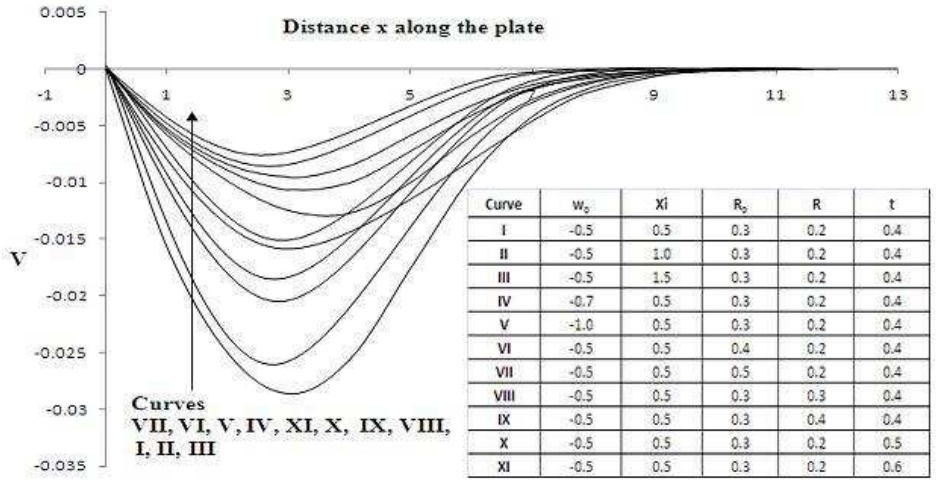

Curve	w_o	Xi	R_o	R	t
I	-0.5	0.5	0.3	0.2	0.4
II	-0.5	1.0	0.3	0.2	0.4
III	-0.5	1.5	0.3	0.2	0.4
IV	-0.7	0.5	0.3	0.2	0.4
V	-1.0	0.5	0.3	0.2	0.4
VI	-0.5	0.5	0.4	0.2	0.4
VII	-0.5	0.5	0.5	0.2	0.4
VIII	-0.5	0.5	0.3	0.3	0.4
IX	-0.5	0.5	0.3	0.4	0.4
X	-0.5	0.5	0.3	0.2	0.5
XI	-0.5	0.5	0.3	0.2	0.6

Figure 15: Secondary velocity profiles when w_o, Xi, Ro, R, and t are varied.

International Electronic Journal of Pure and Applied Mathematics – IEJPAM, Volume 4, No. 4 (2012)

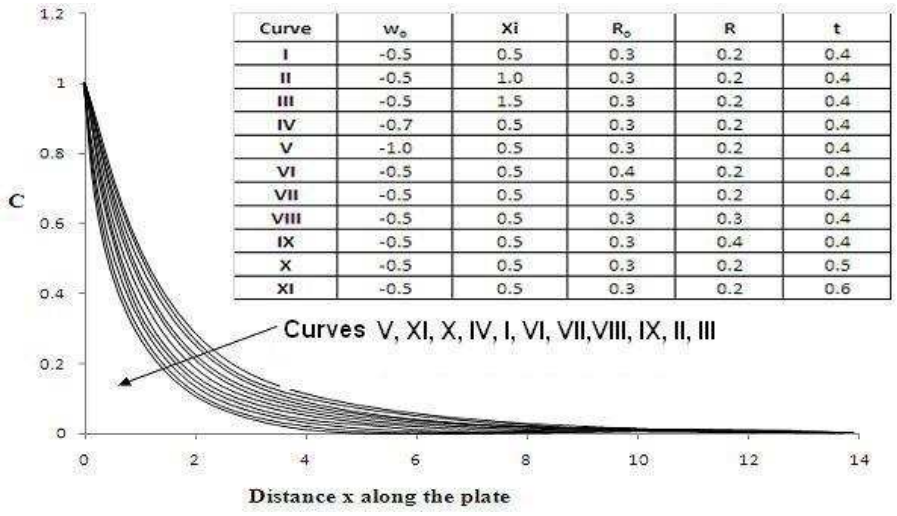

Figure 16: Concentration profiles when w_o, Xi, Ro, R, and t are varied.

International Electronic Journal of Pure and Applied Mathematics – IEJPAM, Volume 4, No. 4 (2012)

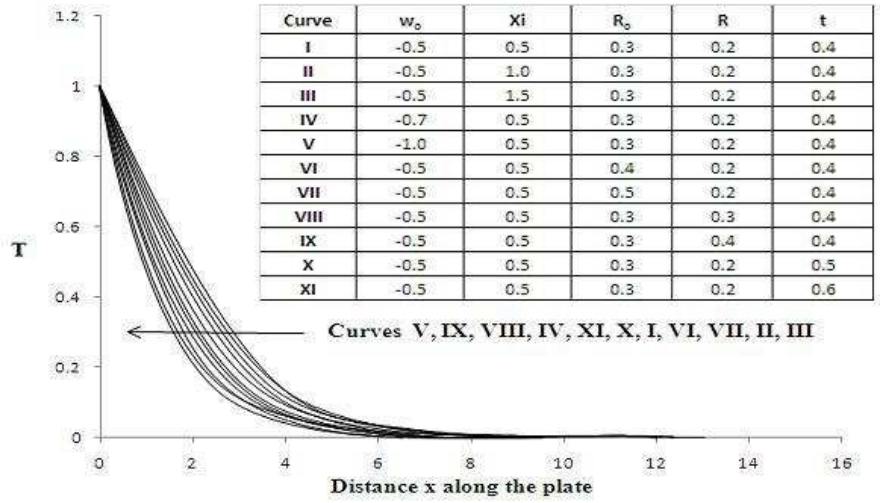

Figure 17: Temperature profiles when w_o, Xi, Ro, R, and t are varied.